INORGANIC CHEMISTRY FRONTIERS

RESEARCH ARTICLE

View Article Online
View Journal | View Issue

Cite this: *Inorg. Chem. Front.*, 2025, **12**, 5328

Strong NIR electrochemiluminescence from lanthanide ions sensitized with a carbon-rich ruthenium chelate†

Jing Yu,‡[a,b] Miaoxia Liu,‡[b] Tuan-Anh Phan,[c] Laurent Bouffier,[b] Lucie Norel,[c,d] Stephane Rigaut *[c] and Neso Sojic *[a,b]

Received 15th February 2025,
Accepted 23rd April 2025

DOI: 10.1039/d5qi00450k

rsc.li/frontiers-inorganic

We report on intense electrochemiluminescence (ECL) emission from the redox switching of a series of heterobimetallic systems consisting of lanthanide complexes emitting in the near-infrared (NIR) range (Yb^{3+} and Nd^{3+}) associated with a redox-active carbon-rich ruthenium bipyridyl antenna chelate. The NIR ECL emission was achieved successfully using the same molecular scaffold. Electrochemical reactions between the antenna and the sacrificial ECL coreactant allow for the low-potential redox modulation of the NIR luminescence from Yb^{3+} and Nd^{3+}. This strategy offers interesting new insights into NIR ECL systems based on inorganic complexes.

Introduction

Electrochemiluminescence (ECL) is the light emitted from the excited state of a dye initiated by an electrochemical reaction.[1–3] Due to the orthogonality of the initial electrochemical trigger and the final optical readout, ECL offers several advantages such as high sensitivity and selectivity, precise control over the emission position, no use of external light sources, and no photobleaching or phototoxicity.[4–6] It has progressively become a powerful technique for clinical diagnostics and imaging of biological entities and chemical systems.[7–12] Nowadays, the classical ECL system, composed of tris(2,2′-bipyridyl) ruthenium(II) dye, $[Ru(bpy)_3]^{2+}$, and tri-*n*-propylamine (TPrA) coreactant, is a benchmark for visible range emission (615 nm).[7,13–15] However, a major experimental effort also focusses on the development of new ECL-active dyes emitting in the NIR region to extend the potentialities of ECL technology, within the biologically transparent window.[16–33]

The possibility of combining this feature with sharp emission bands for multiplexed ECL detection makes lanthanide-based systems particularly attractive.[28,34–45] Indeed, lanthanide-based (Yb^{3+}, Nd^{3+}, Eu^{3+}, *etc.*) complexes display long-lived, well-defined, and narrow bandwidth photoluminescence (PL) bands ranging from the visible to the NIR spectral range, with high emission efficiency, particularly attractive for biological applications.[46] For such complexes, sensitization with a chromophore able to transfer its excited state energy to one of the lanthanides is needed because direct excitation corresponds to forbidden transitions.[36,47–50] The sensitization process can proceed *via* either electron transfer or energy transfer from an excited antenna ligand.[51,52] In the case of NIR emitters, chromophores with visible absorption, such as tetrathiafulvalene, ferrocene,[50,53] and metal acetylide complexes,[49,54,55] are particularly suitable and also exhibit accessible redox events for luminescence switching.[56] Among them, ruthenium acetylide complexes, which belong to group-8 metal complexes, are attractive redox-switchable building blocks with oxidation potential similar to that of ferrocene. In addition, they exert strong ligand-mediated electronic effects owing to the substantial ligand character of the highest occupied molecular orbital (HOMO) resulting from the overlap of a metal d(π) orbital with an appropriate π orbital of the carbon-rich ligand, leading to a major involvement of this ligand in the redox processes and a minor metal contribution.[49] In this context, it has been demonstrated that ruthenium acetylide complexes with chelating units can modulate Nd(III) and Yb(III) PL successfully by a simple redox process.[49,54,55] However, surprisingly, to our knowledge, ECL has not been achieved so far with such a heterobimetallic scaffold in coreactant ECL and, more generally, it has not been achieved with lanthanide NIR emitters.

Herein, ECL from a series of lanthanide complexes with NIR luminescence (Scheme 1) is demonstrated by taking advantage of the redox trigger of the abovementioned and pre-

[a]*College of Chemistry and Chemical Engineering, Yantai University, 264005 Yantai, China*
[b]*Univ. Bordeaux, CNRS UMR 5255, Bordeaux INP, ENSMAC, 33607 Pessac, France. E-mail: sojic@u-bordeaux.fr*
[c]*Univ. Rennes, CNRS, ISCR (Institut des Sciences Chimiques de Rennes) – UMR 6226, F-35000 Rennes, France. E-mail: stephane.rigaut@univ-rennes.fr*
[d]*Institut Universitaire de France, France*

†Electronic supplementary information (ESI) available. See DOI: https://doi.org/10.1039/d5qi00450k

‡These authors contributed equally to this work.

viously synthesized carbon-rich ruthenium complexes *trans*-[Ph–C≡C –(dppe)$_2$Ru–C≡C–bpy-κ^2*N*,*N*′–Ln(TTA)$_3$] (**1Ru–Ln**, where Ln = Yb and Nd, dppe = 1,2-bis-(diphenylphosphinyl) ethane and TTA = 2-thenoyltrifluoro-acetonate),[49,55] *via* the coreactant ECL pathway. The excited state of the ruthenium antenna is likely generated through an electrochemical reaction with TPrA in a wide potential range, followed by the sensitization of lanthanide ions coordinated with the bipyridine ligand. The separated moiety Yb(TTA)$_3$(phen) (with phen = phenanthroline) named **2Yb** and the ruthenium acetylide complex (**3Ru**) were also employed for control experiments.

Results and discussion

Since the ECL process is governed by electrochemistry and both homogeneous and heterogeneous electron-transfer reactions, the electrochemical properties of the **1Ru–Ln** series were investigated by cyclic voltammetry (CV) in a degassed CH_2Cl_2 solution containing 0.2 M $TBAPF_6$ as a supporting electrolyte as well as both monometallic moieties **2Yb** and **3Ru**, respectively (Scheme 1). The heterobimetallic complex **1Ru–Yb** was first studied and displays a reversible one-electron anodic wave peaking at 0.56 V *vs.* the Ag pseudo-reference electrode (Fig. 1a), corresponding to the reversible oxidation of the carbon-rich ruthenium antenna moiety. The **3Ru** complex, which comprised only the ruthenium acetylide center without the electron-withdrawing lanthanide center, showed the same oxidation wave (Fig. S1a†). **1Ru–Nd** exhibited the same reversible oxidation wave (Fig. S2†), confirming the attribution of this reversible one-electron transfer reaction to the ruthenium moiety.[49] The anodic peak current of the first reversible oxidation wave is slightly smaller for **1Ru–Nd** in comparison with **3Ru**. Such a difference reflects the larger size of **1Ru–Nd** compared to **3Ru**, which directly affects the corresponding diffusion coefficient. At higher anodic potentials, the CVs of **1Ru–Yb** showed an irreversible process at 1.25 V, similar to the **1Ru–Nd** complex (Fig. S2†). These results are consistent with the voltammetric behaviour reported in the literature.[49] In comparison, the lanthanide moiety (*i.e.* **2Yb**) exhibited an irreversible oxidation process with an onset potential at 1.65 V (Fig. S3†),[34] but we should mention that the ligand in **2Yb** was phenanthroline, whereas it was a bipyridyl ligand in **1Ru–Ln**. However, we consider that such a small structural change does not significantly affect the interpretation of the voltammetric results and that they remain valid in a first-order approximation.

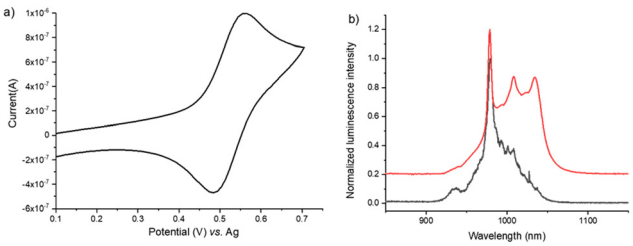

Fig. 1 (a) Cyclic voltammogram of 0.5 mM **1Ru–Yb** in a degassed CH_2Cl_2 solution with 0.2 M $TBAPF_6$ as a supporting electrolyte. Scan rate: 0.05 V s^{-1}. (b) Normalized ECL (black line) and photo-excited emission (red line) spectra of **1Ru–Yb**. The ECL spectrum was recorded in a CH_2Cl_2 solution containing 0.5 mM **1Ru–Yb**, 100 mM TPrA and 0.2 M $TBAPF_6$. A Pt disk and an Ag wire were used as the working electrode and the pseudo-reference electrode, respectively. For the sake of clarity to distinguish both spectra, the PL (λ_{exc} = 450 nm) signal was translated vertically by an increment of 0.2.

Since **1Ru–Yb** exhibited a reversible electron-transfer reaction in oxidation, we used an anodic sacrificial coreactant to probe the possibility of generating its excited state rather than by an annihilation mechanism.[2] The role of this coreactant is to produce a highly reducing species that can populate the excited state of the dye by a sufficiently exergonic electron-transfer reaction with the oxidized species **[1Ru–Yb]**$^+$. In this study, we selected the highly efficient TPrA coreactant, which is widely used to promote the ECL of the archetypical [Ru(bpy)$_3$]$^{2+}$ dye and others for numerous applications in analytical chemistry and microscopy.[11,57–60] The ECL process follows the "oxidative-reduction" mechanism occurring by simply applying an anodic potential sweep or step to oxidize both the coreactant and the dye at the electrode surface. After a fast deprotonation of the electrogenerated TPrA$^{\bullet+}$ cation radical, the neutral strong reductant TPrA$^{\bullet}$ radical is produced. It reacts with the oxidized form of the dye and generates its excited state. Using such an "oxidative-reduction" pathway, we successfully recorded the ECL spectrum of **1Ru–Yb**. Fig. 1b shows the ECL spectrum (black line) and the comparison with the PL spectrum (red line) of **1Ru–Yb** previously obtained by photo-excitation with the low-energy metal-to-ligand charge transfer (MLCT) transition corresponding to transitions from Ru(dπ)/alkynyl-based orbitals to a π* orbital associated with the bipyridine unit.[49,54] It is noteworthy that the ECL spectra were obtained using an optic fibre spectrometer equipped with a silicon-based CCD detector whose quantum efficiency vanishes drastically in the NIR range after 850 nm, explaining a well-known spectral discrepancy in comparison with that obtained with an InGaAs detector for the PL spectra (see the ESI for details on the photodetectors†).[61] Overall, the same

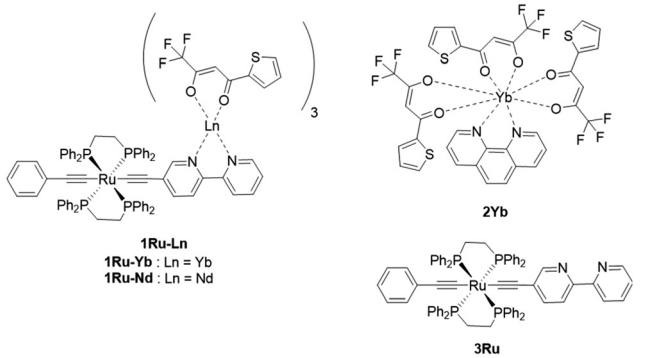

Scheme 1 Chemical structures of complexes **1Ru–Ln** (Ln = Yb or Nd), **2Yb** and **3Ru**.

intense characteristic line shape of Yb(III) at 980 nm ($2F_{5/2} \rightarrow 2F_{7/2}$) was observed both in ECL and in PL, indicating the formation of the same excited state. Therefore, we can conclude that ECL probably proceeded through the sensitization mechanism from the Ru acetylide ligand to the Yb(III) ion with the help of an intramolecular energy transfer from the carbon-rich antenna to the metal ion (*vide infra*).

Then, we further investigated the effect of the imposed anodic potential on the ECL signal of the heterobimetallic **1Ru–Yb** complex in the presence of TPrA. ECL spectra were obtained using multistep chronoamperometric mode by applying progressively higher potential values (Fig. 2a). The ECL spectra with a sharp peak at 980 nm can be observed for potentials higher than 0.6 V. We calculated the global ECL signal by integrating the area under each ECL spectrum and plotted it as a function of the applied potential (Fig. 2b) for comparison with the current recorded during the voltammetric scan. The strength of the ECL signal was found to be correlated to the current with an onset potential of around 0.6 V and then an increase with a maximum at 1.6 V. One can see a clear correlation between the oxidation current and the ECL emission, which is self-consistent. The current intensity is mainly dominated by the oxidation of TPrA since, as classically performed in ECL studies, the coreactant concentration is largely in excess (*i.e.*, 100 mM) compared to the concentration of the dye (*i.e.*, 0.5 mM). Thus, above 0.6 V, both **1Ru–Yb** and TPrA are oxidized. This indicates that, as expected, the ECL emission of **1Ru–Yb** requires the oxidation of both TPrA and **1Ru–Yb**. However, oxidation of the Yb(III) moiety, which occurs at higher potential, is not necessary to generate the ECL emission of the complex. The maximum values of both the ECL signal and current occur at 1.6 V, after which they decrease rapidly when applying larger overpotentials. This decrease is correlated with the lower oxidation current of TPrA at potentials higher than 1.6 V. From this study, we can conclude that the oxidized carbon-rich ruthenium antenna reacts with the electrogenerated TPrA radicals directly to generate the excited state. This step is followed by intramolecular energy transfer occurring from the excited carbon-rich ruthenium antenna to the Yb(III) ion. Interestingly, ECL can still be observed even at a high applied potential of 2 V (Fig. S4†), indicating that ECL emission of the Yb(III) complex may be generated in a wide potential range. In addition, ECL emission is visible even at potentials where the Yb(III) moiety is oxidized.

We performed a series of control experiments to confirm the ECL mechanism in action. Without TPrA, no ECL signal was observed (Fig. S5a,† orange line), showing that the ECL was generated effectively *via* the coreactant pathway between the heterobimetallic ruthenium carbon-rich Yb(III) complex and TPrA radicals. In addition, under the same experimental conditions, the ECL spectrum of **2Yb** (Fig. S5b,† green line) displayed a very weak peak in the NIR range, confirming the essential role of the antenna in efficiently sensitizing the Yb (III) luminescence. Similarly, there was no ECL signal in the NIR range when using solely the ruthenium center, **3Ru** (Fig. S5b,† blue line). In addition, both PL and ECL emissions of the Ru moiety at *ca.* 675 nm are quenched by the Ln ion in **1Ru–Ln**. This is self-consistent with previously reported PL results.[55] Importantly, we have to consider that in such a coordinating environment (TPrA), partial decoordination of the Yb (III) ion may occur since the bipyridine unit shows only moderate association constants with lanthanide ions. This possible decoordination has not been considered in previous studies on ECL with lanthanide complexes. In our case, we have carefully checked the amount of decoordinated species, whose absorption spectrum is reminiscent of that of **3Ru**, with a blue shifted MLCT transition located at λ_{max} = 400 nm in comparison with that of **1Ru–Yb** at λ_{max} = 450 nm (see Fig. S6 and the ESI for details†). We could conclude that a major proportion of **1Ru–Yb**, *ca.* 66%, still exists in the ECL medium. In addition, as no significant ECL emission was observed with **2Yb**, the ECL signal observed with **1Ru–Yb** can be unambiguously ascribed to the bimetallic complex.

To probe the potential extension of the reported approach to other lanthanides, the ECL spectrum of another heterobimetallic system (Scheme 1) with Nd^{3+} (**1Ru–Nd**) was also obtained under the same experimental conditions. Fig. 3 shows the comparison of the ECL spectrum (black line) with the photo-excited luminescence spectra at room temperature (red line) and at 77 K in a frozen organic glass (blue line) of **1Ru–Nd**. The latter shows, in particular, the characteristic line sharp emission bands of the Nd(III) ion at 875 nm, 886 nm, 893 nm and 910 nm to the straightforward sensitization mechanism from the Ru acetylide ligand (λ_{exc} = 450 nm). When applying an anodic potential of 1.9 V, a sharp NIR ECL emission band appeared at 875 nm ascribed to the line shaped $^4F_{3/2}$ excited state of Nd(III), with the other transitions at 1063 nm ($^4F_{3/2} \rightarrow {}^4I_{11/2}$) and 1333 nm ($^4F_{3/2} \rightarrow {}^4I_{13/2}$) being, respectively, partially (broad) or totally obliterated by the silicon photodetector (*vide supra*). As in the case of the **1Ru–Yb** complex, at low potentials, a weak ECL emission can be nearly seen, which then increases and reached a maximum at a potential of 1.9 V (Fig. S7a and b†). This demonstrates that the ECL emission from the Nd(III) luminescence can also be sensitized by the excited state of the carbon-rich ruthenium

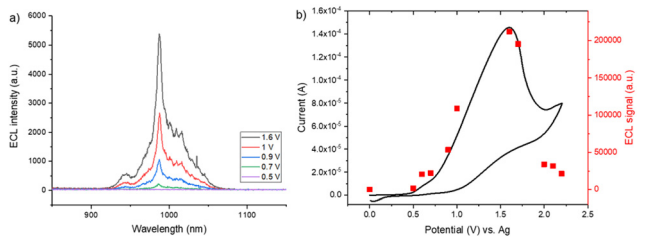

Fig. 2 (a) Evolution of the ECL spectra of **1Ru–Yb** as a function of the imposed potential. (b) Cyclic voltammogram (black line) and corresponding ECL signal (red squares) recorded in a CH_2Cl_2 solution containing 0.5 mM **1Ru–Yb**, 100 mM TPrA and 0.2 M $TBAPF_6$. Scan rate: 0.05 V s^{-1}. The ECL signals (red squares) have been calculated by recording the ECL spectra at different constant potentials and integrating the emission from 900 nm to 1100 nm.

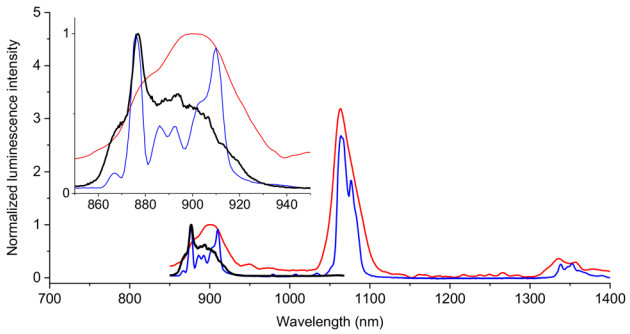

Fig. 3 Comparison of the normalized ECL (black line) and PL emission spectra of **1Ru–Nd** at room temperature (red line, λ_{exc} = 450 nm) and at 77 K in frozen organic glass (blue line) with the same experimental conditions as in Fig. 2. The ECL spectra of **1Ru–Nd** were recorded at an imposed potential of 1.9 V. The inset shows a zoomed-in view of the 850–950 nm area.

antenna generated through the electro-excited process in the presence of TPrA.

To summarize, we demonstrated that ECL emission is possible in the NIR range with Ln ions from this series of heterobimetallic **1Ru–Ln** complexes that can be generated efficiently in oxidation. The ECL mechanism of **1Ru–Ln** follows the "oxidative-reduction" pathway[7,62] *via* the Ru antenna and can be described as follows:

$$\mathbf{1Ru–Ln} \rightarrow \mathbf{1Ru^{+}–Ln} + e^{-} \quad (1)$$

$$TPrA \rightarrow TPrA^{\bullet+} + e^{-} \quad (2)$$

$$TPrA^{\bullet+} \rightarrow TPrA^{\bullet} + H^{+} \quad (3)$$

$$\mathbf{1Ru^{+}–Ln} + TPrA^{\bullet} \rightarrow \mathbf{1Ru*–Ln} + P \quad (4)$$

$$\mathbf{1Ru*–Ln} \rightarrow \mathbf{1Ru–Ln*} \quad (5)$$

$$\mathbf{1Ru–Ln*} \rightarrow \mathbf{1Ru–Ln} + h\nu \quad (6)$$

with P being an iminium product.

Both the dye and coreactant are oxidized directly at the electrode surface (eqn (1) and (2)), which is not possible in the case of **2Yb**. After deprotonation (eqn (3)), the neutral TPrA radical reacts exergonically with the oxidized dye and forms the excited state of the ruthenium moiety (eqn (4)), which sensitizes the Nd(III) or the Yb(III) lanthanide centers (eqn (5)) *via* energy transfer, while an electron transfer process is also likely with the Yb(III) center (*i.e.* $\mathbf{1Ru^{*}}–Yb^{III} \rightarrow \mathbf{1Ru^{+}}–Yb^{II} \rightarrow \mathbf{1Ru}–Yb^{III*}$ for eqn (5)).[63,64] Finally, from the lanthanide-centered excited state, the characteristic sharp luminescence in the NIR range is emitted (eqn (6)). Scheme 2 shows a qualitative energy diagram based on the excited state energy levels and ECL/PL processes.

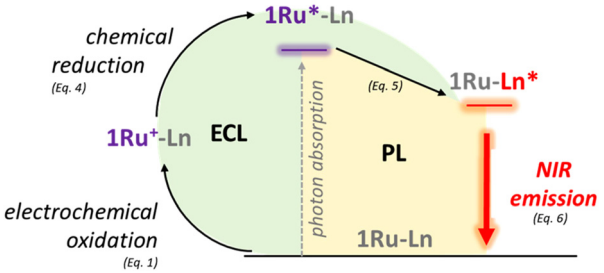

Scheme 2 Energy diagram based on the excited state energy levels and the ECL and PL processes.

Conclusion

Our study demonstrated strong ECL signals originating from a series of heterobimetallic complexes comprising a ruthenium acetylide antenna conjugated to an NIR emissive lanthanide (Yb and Nd) unit *via* a bipyridyl ligand. The characteristic ECL emissions of the lanthanides in the NIR spectral range were achieved by populating first the excited state of the ruthenium acetylide moiety by the coreactant "oxidative-reduction" pathway, which transfers its energy to the lanthanide moiety. The electrochemical control of ECL emission using such chemically engineered heterobimetallic complexes can attract considerable interest for imaging or other analytical applications.

Data availability

The data supporting this article have been included as part of the ESI† and are available upon request to the authors.

Conflicts of interest

There are no conflicts to declare.

Acknowledgements

The authors thank the China Scholarship Council and the Agence Nationale de la Recherche (E-POLAR, ANR-24-CE29-2108-02 and 2LCDOR, ANR-21-CE07-0063-01).

References

1 Z. Liu, W. Qi and G. Xu, Recent advances in electrochemiluminescence, *Chem. Soc. Rev.*, 2015, **44**, 3117–3142.
2 M. Hesari and Z. Ding, Review—Electrogenerated Chemiluminescence: Light Years Ahead, *J. Electrochem. Soc.*, 2016, **163**, H3116–H3131.
3 G. Valenti, E. Rampazzo, S. Kesarkar, D. Genovese, A. Fiorani, A. Zanut, F. Palomba, M. Marcaccio, F. Paolucci and L. Prodi, Electrogenerated chemiluminescence from

metal complexes-based nanoparticles for highly sensitive sensors applications, *Coord. Chem. Rev.*, 2018, **367**, 65–81.
4 H. Qi and C. Zhang, Electrogenerated Chemiluminescence Biosensing, *Anal. Chem.*, 2020, **92**, 524–534.
5 C. Ma, Y. Cao, X. Gou and J.-J. Zhu, Recent Progress in Electrochemiluminescence Sensing and Imaging, *Anal. Chem.*, 2020, **92**, 431–454.
6 X. Ma, W. Gao, F. Du, F. Yuan, J. Yu, Y. Guan, N. Sojic and G. Xu, Rational Design of Electrochemiluminescent Devices, *Acc. Chem. Res.*, 2021, **54**, 2936–2945.
7 S. Rebeccani, A. Zanut, C. I. Santo, G. Valenti and F. Paolucci, A Guide Inside Electrochemiluminescent Microscopy Mechanisms for Analytical Performance Improvement, *Anal. Chem.*, 2021, **94**, 336–348.
8 A. Barhoum, Z. Altintas, K. S. S. Devi and R. J. Forster, Electrochemiluminescence biosensors for detection of cancer biomarkers in biofluids: Principles, opportunities, and challenges, *Nano Today*, 2023, **50**, 101874.
9 J. Totoricaguena-Gorriño, M. Dei, A. F. Alba, N. Peřinka, L.-R. Rubio, J. L. Vilas-Vilela and F. J. del Campo, Toward Next-Generation Mobile Diagnostics: Near-Field Communication-Powered Electrochemiluminescent Detection, *ACS Sens.*, 2022, **7**, 1544–1554.
10 Y. Wang, R. Jin, N. Sojic, D. Jiang and H.-Y. Chen, Intracellular Wireless Analysis of Single Cells by Bipolar Electrochemiluminescence Confined in a Nanopipette, *Angew. Chem., Int. Ed.*, 2020, **59**, 10416–10420.
11 N. Sojic, S. Knežević, D. Han, B. Liu and D. Jiang, Electrochemiluminescence Microscopy, *Angew. Chem., Int. Ed.*, 2024, **63**, e202407588.
12 J. Zhang, S. Arbault, N. Sojic and D. Jiang, Electrochemiluminescence Imaging for Bioanalysis, *Annu. Rev. Anal. Chem.*, 2019, **12**, 275–295.
13 M. Sornambigai, L. Bouffier, N. Sojic and S. S. Kumar, Tris (2,2′-bipyridyl)ruthenium(II) complex as a universal reagent for the fabrication of heterogeneous electrochemiluminescence platforms and its recent analytical applications, *Anal. Bioanal. Chem.*, 2023, **415**, 5875–5898.
14 Y. Yuan, S. Han, L. Hu, S. Parveen and G. Xu, Coreactants of tris(2,2′-bipyridyl)ruthenium(II) Electrogenerated Chemiluminescence, *Electrochim. Acta*, 2012, **82**, 484–492.
15 F. Du, Y. Chen, C. Meng, B. Lou, W. Zhang and G. Xu, Recent advances in electrochemiluminescence immunoassay based on multiple-signal strategy, *Curr. Opin. Electrochem.*, 2021, **28**, 100725.
16 Y. Zhao, L. Bouffier, G. Xu, G. Loget and N. Sojic, Electrochemiluminescence with semiconductor (nano) materials, *Chem. Sci.*, 2022, **13**, 2528–2550.
17 S. Carrara, P. Nguyen, L. D'Alton and C. F. Hogan, Electrochemiluminescence energy transfer in mixed iridium-based redox copolymers immobilised as nanoparticles, *Electrochim. Acta*, 2019, **313**, 397–402.
18 M. Majuran, G. Armendariz-Vidales, S. Carrara, M. A. Haghighatbin, L. Spiccia, P. J. Barnard, G. B. Deacon, C. F. Hogan and K. L. Tuck, Near-Infrared Electrochemiluminescence from Bistridentate Ruthenium (II) Di(quinoline-8-yl)pyridine Complexes in Aqueous Media, *ChemPlusChem*, 2020, **85**, 346–352.
19 L. D'Alton, P. Nguyen, S. Carrara and C. F. Hogan, Intense near-infrared electrochemiluminescence facilitated by energy transfer in bimetallic Ir-Ru metallopolymers, *Electrochim. Acta*, 2021, **379**, 138117.
20 G. Armendariz-Vidales, P. Ramkissoon, P. J. Barnard and C. F. Hogan, Potential-controlled visible and near-infrared electrochemiluminescence from a BODIPY-DO3A macrocycle conjugate, *Electrochim. Acta*, 2023, **468**, 143144.
21 H. Li, A. Wallabregue, C. Adam, G. M. Labrador, J. Bosson, L. Bouffier, J. Lacour and N. Sojic, Bright Electrochemiluminescence Tunable in the Near-Infrared of Chiral Cationic Helicene Chromophores, *J. Phys. Chem. C*, 2017, **121**, 785–792.
22 R. R. Maar, R. Zhang, D. G. Stephens, Z. Ding and J. B. Gilroy, Near-Infrared Photoluminescence and Electrochemiluminescence from a Remarkably Simple Boron Difluoride Formazanate Dye, *Angew. Chem., Int. Ed.*, 2019, **58**, 1052–1056.
23 J.-L. Liu, J.-Q. Zhang, Z.-L. Tang, Y. Zhuo, Y.-Q. Chai and R. Yuan, Near-infrared aggregation-induced enhanced electrochemiluminescence from tetraphenylethylene nanocrystals: a new generation of ECL emitters, *Chem. Sci.*, 2019, **10**, 4497–4501.
24 L. Fu, K. Fu, X. Gao, S. Dong, B. Zhang, S. Fu, H.-Y. Hsu and G. Zou, Enhanced Near-Infrared Electrochemiluminescence from Trinary Ag–In–S to Multinary Ag–Ga–In–S Nanocrystals via Doping-in-Growth and Its Immunosensing Applications, *Anal. Chem.*, 2021, **93**, 2160–2165.
25 L. Yu, Q. Zhang, Q. Kang, B. Zhang, D. Shen and G. Zou, Near-Infrared Electrochemiluminescence Immunoassay with Biocompatible Au Nanoclusters as Tags, *Anal. Chem.*, 2020, **92**, 7581–7587.
26 M. Hesari and Z. Ding, Efficient Near-Infrared Electrochemiluminescence from Au_{18} Nanoclusters, *Chem. – Eur. J.*, 2021, **27**, 14821–14825.
27 M. Hesari and Z. Ding, Identifying Highly Photoelectrochemical Active Sites of Two Au_{21} Nanocluster Isomers toward Bright Near-Infrared Electrochemiluminescence, *J. Am. Chem. Soc.*, 2021, **143**, 19474–19485.
28 N. Gao, B. Ling, Z. Gao, L. Wang and H. Chen, Near-infrared-emitting NaYF4:Yb,Tm/Mn upconverting nanoparticle/gold nanorod electrochemiluminescence resonance energy transfer system for sensitive prostate-specific antigen detection, *Anal. Bioanal. Chem.*, 2017, **409**, 2675–2683.
29 L. Jiang, M. Jing, B. Yin, W. Du, X. Wang, Y. Liu, S. Chen and M. Zhu, Bright near-infrared circularly polarized electrochemiluminescence from Au_9Ag_4 nanoclusters, *Chem. Sci.*, 2023, **14**, 7304–7309.
30 R. Ishimatsu, H. Shintaku, Y. Kage, M. Kamioka, S. Shimizu, K. Nakano, H. Furuta and T. Imato, Efficient Electrogenerated Chemiluminescence of Pyrrolopyrrole Aza-BODIPYs in the Near-Infrared Region with

Tripropylamine: Involving Formation of S2 and T2 States, *J. Am. Chem. Soc.*, 2019, **141**, 11791–11795.

31 H.-J. Lu, J.-J. Xu, H. Zhou and H.-Y. Chen, Recent advances in electrochemiluminescence resonance energy transfer for bioanalysis: Fundamentals and applications, *TrAC, Trends Anal. Chem.*, 2020, **122**, 115746.

32 S.-Y. Ji, J.-B. Pan, H.-Z. Wang, W. Zhao, H.-Y. Chen and J.-J. Xu, Highly Efficient Near-Infrared II Electrochemiluminescence from $NaYbF_4$ Core Mesoporous Silica Shell Nanoparticles, *CCS Chem.*, 2022, **4**, 3076–3083.

33 H. Gao, J.-B. Lin, S.-M. Wang, Q.-Q. Tao, B.-Z. Tang, H.-Y. Chen and J.-J. Xu, Near-infrared II aggregation-induced electrochemiluminescence of organic dots, *Chem. Commun.*, 2024, **60**, 562–565.

34 R. Ishimatsu, E. Kunisawa, K. Nakano, C. Adachi and T. Imato, Electrogenerated Chemiluminescence and Electronic States of Several Organometallic Eu(III) and Tb (III) Complexes: Effects of the Ligands, *ChemistrySelect*, 2019, **4**, 2815–2831.

35 E. Kunisawa, R. Ishimatsu, K. Nakano and T. Imato, Electrogenerated Chemiluminescence of Tris(dibenzoylmethane)phenanthroline Europium(III) as a Light Source: An Application for the Detection of PO_4^{3-} Based on the Ion Associate Formation of Phosphomolybdic Acid and Malachite Green, *Anal. Sci.*, 2019, **35**, 799–802.

36 B. D. Stringer, L. M. Quan, P. J. Barnard and C. F. Hogan, Electrochemically Sensitized Luminescence from Lanthanides in d-/f-Block Heteronuclear Arrays, *ChemPhotoChem*, 2018, **2**, 27–33.

37 H.-X. Yu, H. Cui and J.-B. Guan, Cathodic electrochemiluminescence of acetonitrile, acetonitrile–1,10-phenanthroline and acetonitrile–ternary Eu(III) complexes at a gold electrode, *Luminescence*, 2006, **21**, 81–89.

38 C. Wang, Z. Li and H. Ju, Copper-Doped Terbium Luminescent Metal Organic Framework as an Emitter and a Co-reaction Promoter for Amplified Electrochemiluminescence Immunoassay, *Anal. Chem.*, 2021, **93**, 14878–14884.

39 Q. Han, C. Wang, P. Liu, G. Zhang, L. Song and Y. Fu, Functionalized europium-porphyrin coordination polymer: Rational design of high performance electrochemiluminescence emitter for mucin 1 sensing, *Biosens. Bioelectron.*, 2021, **191**, 113422.

40 K. Chen, J. Liu, G. Shu, Y. Yang, Y. Zhu and G. Zhao, Electrochemiluminescence of terbium(III) complex and its potential application for the determination of bacterial endospores, *J. Lumin.*, 2013, **141**, 71–75.

41 L. Deng, Y. Shan, J.-J. Xu and H.-Y. Chen, Electrochemiluminescence behaviors of Eu3+-doped CdS nanocrystals film in aqueous solution, *Nanoscale*, 2012, **4**, 831–836.

42 X. Zhuang, X. Gao, C. Tian, D. Cui, F. Luan, Z. Wang, Y. Xiong and L. Chen, Synthesis of europium(iii)-doped copper nanoclusters for electrochemiluminescence bioanalysis, *Chem. Commun.*, 2020, **56**, 5755–5758.

43 M. Liu, Y. Ye, C. Yao, W. Zhao and X. Huang, Mn^{2+}-doped $NaYF_4$:Yb/Er upconversion nanoparticles with amplified electrogenerated chemiluminescence for tumor biomarker detection, *J. Mater. Chem. B*, 2014, **2**, 6626–6633.

44 X. Guo, S. Wu, N. Duan and Z. Wang, Mn^{2+}-doped $NaYF_4$: Yb/Er upconversion nanoparticle-based electrochemiluminescent aptasensor for bisphenol A, *Anal. Bioanal. Chem.*, 2016, **408**, 3823–3831.

45 Y. Zhou, Z. Mao and J.-J. Xu, Recent advances in near infrared (NIR) electrochemiluminescence luminophores, *Chin. Chem. Lett.*, 2024, **35**, 109622.

46 S. V. Eliseeva and J.-C. G. Bünzli, Lanthanide luminescence for functional materials and bio-sciences, *Chem. Soc. Rev.*, 2010, **39**, 189–227.

47 M. M. Richter and A. J. Bard, Electrogenerated Chemiluminescence. 58. Ligand-Sensitized Electrogenerated Chemiluminescence in Europium Labels, *Anal. Chem.*, 1996, **68**, 2641–2650.

48 D. Pinjari, A. Z. Alsaleh, Y. Patil, R. Misra and F. D'Souza, Interfacing High-Energy Charge-Transfer States to a Near-IR Sensitizer for Efficient Electron Transfer upon Near-IR Irradiation, *Angew. Chem., Int. Ed.*, 2020, **59**, 23697–23705.

49 E. Di Piazza, L. Norel, K. Costuas, A. Bourdolle, O. Maury and S. Rigaut, d–f Heterobimetallic Association between Ytterbium and Ruthenium Carbon-Rich Complexes: Redox Commutation of Near-IR Luminescence, *J. Am. Chem. Soc.*, 2011, **133**, 6174–6176.

50 M. Tropiano, N. L. Kilah, M. Morten, H. Rahman, J. J. Davis, P. D. Beer and S. Faulkner, Reversible Luminescence Switching of a Redox-Active Ferrocene–Europium Dyad, *J. Am. Chem. Soc.*, 2011, **133**, 11847–11849.

51 L. Armelao, S. Quici, F. Barigelletti, G. Accorsi, G. Bottaro, M. Cavazzini and E. Tondello, Design of luminescent lanthanide complexes: From molecules to highly efficient photo-emitting materials, *Coord. Chem. Rev.*, 2010, **254**, 487–505.

52 Y. Hasegawa, Y. Kitagawa and T. Nakanishi, Effective photosensitized, electrosensitized, and mechanosensitized luminescence of lanthanide complexes, *NPG Asia Mater.*, 2018, **10**, 52–70.

53 B. Lefeuvre, J. Flores Gonzalez, F. Gendron, V. Dorcet, F. Riobé, V. Cherkasov, O. Maury, B. Le Guennic, O. Cador, V. Kuropatov and F. Pointillart, Redox-Modulations of Photophysical and Single-molecule Magnet Properties in Ytterbium Complexes Involving Extended-TTF Triads, *Molecules*, 2020, **25**, 492.

54 H. Al Sabea, L. Norel, O. Galangau, H. Hijazi, R. Métivier, T. Roisnel, O. Maury, C. Bucher, F. Riobé and S. Rigaut, Dual Light and Redox Control of NIR Luminescence with Complementary Photochromic and Organometallic Antennae, *J. Am. Chem. Soc.*, 2019, **141**, 20026–20030.

55 L. Norel, E. Di Piazza, M. Feng, A. Vacher, X. He, T. Roisnel, O. Maury and S. Rigaut, Lanthanide Sensitization with Ruthenium Carbon-Rich Complexes and Redox Commutation of Near-IR Luminescence, *Organometallics*, 2014, **33**, 4824–4835.

56 L. Norel, O. Galangau, H. Al Sabea and S. Rigaut, Remote Control of Near Infrared Emission with Lanthanide Complexes, *ChemPhotoChem*, 2021, **5**, 393–405.
57 E. Kerr, E. H. Doeven, D. J. D. Wilson, C. F. Hogan and P. S. Francis, Considering the chemical energy requirements of the tri-n-propylamine co-reactant pathways for the judicious design of new electrogenerated chemiluminescence detection systems, *Analyst*, 2016, **141**, 62–69.
58 S. Knežević, E. Kerr, B. Goudeau, G. Valenti, F. Paolucci, P. S. Francis, F. Kanoufi and N. Sojic, Bimodal Electrochemiluminescence Microscopy of Single Cells, *Anal. Chem.*, 2023, **95**, 7372–7378.
59 D. Han, D. Fang, G. Valenti, F. Paolucci, F. Kanoufi, D. Jiang and N. Sojic, Dynamic mapping of electrochemiluminescence reactivity in space: application to bead-based assays, *Anal. Chem.*, 2023, **95**, 15700–15706.
60 D. Han, D. Jiang, G. Valenti, F. Paolucci, F. Kanoufi, P. C. Chaumet, D. Fang and N. Sojic, Optics Determines the Electrochemiluminescence Signal of Bead-Based Immunoassays, *ACS Sens.*, 2023, **8**, 4782–4791.
61 A. D'Aléo, A. Bourdolle, S. Brustlein, T. Fauquier, A. Grichine, A. Duperray, P. L. Baldeck, C. Andraud, S. Brasselet and O. Maury, Ytterbium-based bioprobes for near-infrared two-photon scanning laser microscopy imaging, *Angew. Chem., Int. Ed.*, 2012, **51**, 6622–6625.
62 C. Mariani, S. Bogialli, F. Paolucci, P. Pastore, A. Zanut and G. Valenti, Enhancing electrochemiluminescence intensity through emission layer control, *Electrochim. Acta*, 2024, **489**, 144256.
63 E. Mathieu, S. R. Kiraev, D. Kovacs, J. A. L. Wells, M. Tomar, J. Andres and K. E. Borbas, Sensitization Pathways in NIR-Emitting Yb(III) Complexes Bearing 0, +1, +2, or +3 Charges, *J. Am. Chem. Soc.*, 2022, **144**, 21056–21067.
64 T. Lazarides, N. M. Tart, D. Sykes, S. Faulkner, A. Barbieri and M. D. Ward, [Ru(bipy)3]2 + and [Os(bipy)3]2 + chromophores as sensitisers for near-infrared luminescence from Yb(iii) and Nd(iii) in d/f dyads: contributions from Förster, Dexter, and redox-based energy-transfer mechanisms, *Dalton Trans.*, 2009, 3971–3979.